

# RSC Advances



This is an *Accepted Manuscript*, which has been through the Royal Society of Chemistry peer review process and has been accepted for publication.

*Accepted Manuscripts* are published online shortly after acceptance, before technical editing, formatting and proof reading. Using this free service, authors can make their results available to the community, in citable form, before we publish the edited article. This *Accepted Manuscript* will be replaced by the edited, formatted and paginated article as soon as this is available.

You can find more information about *Accepted Manuscripts* in the [Information for Authors](#).

Please note that technical editing may introduce minor changes to the text and/or graphics, which may alter content. The journal's standard [Terms & Conditions](#) and the [Ethical guidelines](#) still apply. In no event shall the Royal Society of Chemistry be held responsible for any errors or omissions in this *Accepted Manuscript* or any consequences arising from the use of any information it contains.



## Treatment of Textile Wastewater under Visible LED Lamps using CuO/ZnO Nanoparticles Immobilized on Scoria Rocks

F. Mahdizadeh, S. Aber\*

Received 00th January 20xx,  
Accepted 00th January 20xx

DOI: 10.1039/x0xx00000x  
[www.rsc.org/](http://www.rsc.org/)

ZnO thin film was synthesized by sol-gel method and dip-coated on granular porous natural scoria. CuO nanoparticles were synthesized on ZnO/scoria using a direct crystallization approach in the presence of sodium borohydride. Structure and characterization of ZnO/scoria and CuO/ZnO/scoria nanophotocatalysts were studied by X-ray diffraction (XRD) analysis, energy-dispersive X-ray spectroscopy (EDS), scanning electron microscopy (SEM) and diffuse reflectance spectroscopy (DRS). Photocatalytic decolorization of acid blue 113 and a textile wastewater were performed using the CuO/ZnO/scoria nanophotocatalyst under LED visible lamps in a continuous open channel reactor. Effect of pH, flow rate, initial dye concentration and coexisting anions were investigated. The higher acid blue 113 decolorization efficiency was obtained equal to 62.45% at pH=5, initial dye concentration of 20 mg L<sup>-1</sup> and flow rate of 15 ml min<sup>-1</sup>. For a textile wastewater with initial chemical oxygen demand (COD) of 700 mg L<sup>-1</sup>, 72% COD removal was obtained at pH= 4 and flow rate of 2 ml min<sup>-1</sup>.

### 1. Introduction

Zinc oxide (ZnO) due to its high photosensitivity has attracted tremendous attention as a photocatalyst<sup>1,2</sup>. In this research, ZnO has been selected as photocatalyst because of its high catalytic efficiency, low cost, and non-toxic nature. Unfortunately, due to the large band gap of ZnO, it is not highly efficient under visible light irradiation which restricts its application for industrial purposes<sup>3</sup>, considering the cost and hazards of UV light. UV light constitutes less than 5% of solar irradiation while visible light constitutes more than 43%<sup>4</sup>. Also, charge carrier recombination occurs very fast in ZnO<sup>4</sup>. It is of high importance to separate the electron-hole pairs to increase photon efficiency by reducing electron-hole recombination and to produce visible-light-active photocatalysts<sup>5-7</sup>. The modification of ZnO to produce a visible-light-sensitive photocatalyst is performed by various methods, i.e. doping with some elements, e.g. Se, Co, Cd; coupling with other metal oxides, e.g. WO<sub>3</sub>, Fe<sub>2</sub>O<sub>3</sub>, SiO<sub>2</sub> and SnO<sub>2</sub> to reduce the energy band gap and to extend the absorbance of visible light and also, for electron-hole separation and achieving a photocatalyst with higher activity<sup>4,8-12</sup>. In this study ZnO/CuO was used as visible-light-sensitive photocatalyst. CuO is a p-type semiconductor with a band gap of 2.17 eV with good photocatalytic properties<sup>13</sup>. To make feasible the recovery and recycle of ZnO/CuO photocatalyst, ZnO thin film was

prepared on granular and porous scoria by sol-gel method. Scoria is a volcanic rock that is abundant in many places worldwide including Central America, Asia (Iran, South Korea, etc.), East Africa (Ethiopia, Kenya, etc.) and Europe (Greece, Spain, Turkey, etc.)<sup>14</sup>. Also, it has low cost, high mechanical and chemical stability and porous structure which provides high surface for photocatalyst immobilization and also for photocatalytic treatment process<sup>15</sup>. Then CuO was synthesized on the prepared ZnO/scoria. The CuO/ZnO nanophotocatalyst was used for the treatment of acid blue 113 (AB113) solution and a textile wastewater under LED visible lamps in a continuous open channel reactor.

### 2. Experimental

#### 2.1. Materials

Granular scoria was obtained from Qorveh mine in Kordestan, west of Iran. AB113 was purchased from Sabet Alvand Company, Hamedan, Iran. Zinc acetate dihydrate, oxalic acid, ethanol, CuSO<sub>4</sub>, HNO<sub>3</sub>, NaNO<sub>3</sub>, NaOH, H<sub>2</sub>SO<sub>4</sub>, K<sub>2</sub>Cr<sub>2</sub>O<sub>7</sub>, HgSO<sub>4</sub>, Ag<sub>2</sub>SO<sub>4</sub>, and HCl all were obtained from Merck Company in analytical grade. The textile wastewater containing AB113 with blue color, pH 4.8 ± 0.2, conductivity 3.59 mS cm<sup>-1</sup>, and chemical oxygen demand (COD) 700 mg L<sup>-1</sup> was obtained from Farsh & Patu factory in Tabriz, Iran.

#### 2.2. Measurement of AB113

An AB113 aqueous solution (20 mg L<sup>-1</sup>) was used to plot its absorbance versus wave length in the range of 200-800 nm and 566 nm was found as the maximum absorbance wavelength. At this wave length the absorbance values of different known solutions of

Research Laboratory of Environment Protection Technology, Department of Applied Chemistry, Faculty of Chemistry, University of Tabriz, Tabriz, Iran. E-mail: soheil\_aber@yahoo.com; Fax: + 98 41 33340191; Tel: +98 41 33393153

AB113 were plotted against their concentrations. This calibration curve was used to convert absorbance data to AB113 concentration. The removal efficiency of the dye was defined using Eq. (1):

$$R(\%) = \frac{C_0 - C_t}{C_0} \times 100 \quad (1)$$

where R is dye removal efficiency,  $C_0$  ( $\text{mg L}^{-1}$ ) is initial concentration of dye, and  $C_t$  ( $\text{mg L}^{-1}$ ) is its concentration at time t.

### 2.3. COD measurement

COD values were measured according to closed-reflux colorimetric standard method using a Palintest photometer (INST 7100, England)<sup>16</sup>. Potassium dichromate was used as oxidizing agent. Concentrated sulfuric acid was used to provide the primary digestion catalyst. The secondary catalyst was silver sulfate ( $\text{AgSO}_4$ ). After digesting the samples for two hours at  $150 \pm 2^\circ\text{C}$ , the samples were cooled and COD values were measured using the Palintest photometer. COD removal (%) for each sample was calculated using Eq. (2).

$$\text{COD removal (\%)} = \frac{\text{COD}_{\text{initial}} - \text{COD}_{\text{final}}}{\text{COD}_{\text{initial}}} \times 100 \quad (2)$$

### 2.4. Scoria preparation

Almost spherical scoria samples (approximately 1.0 cm in diameter and 1.5-2.0 g in weight) were washed several times with tap water to remove any dust and then with distilled water. The washed samples were immersed in distilled water for 10 h to remove water-soluble impurities. For further purification, the samples were treated by 0.5 M HCl for 10 h. After that, the scoria samples were washed with distilled water, again and were dried at  $80^\circ\text{C}$  in an oven (Griffin, UK).

### 2.5. Synthesis and characterization of CuO/ZnO/scoria

At the first step, ZnO synthesised and immobilized on scoria by the sol-gel method. The sol-gel dip-coating method is an interesting way to prepare thin films on supports. It is a fast, simple and inexpensive method that does not use any adhesive. Actually the immobilization of thin film on support by sol-gel method is based on the formation of chemical bonds  $-\text{M}-\text{O}-\text{M}'-$ , where M and M' are metallic ions in the film and substrate respectively<sup>17</sup>. In this research, M is Zn and M' mostly is Si or Al, therefore  $-\text{Zn}-\text{O}-\text{Si}-$  or  $-\text{Zn}-\text{O}-\text{Al}-$  was formed through the reaction of Zn-OH group with Si-OH or Al-OH group. Due to this chemical reaction photocatalyst has good adherence with support.

Zinc oxide was prepared by sol-gel method using zinc acetate (0.2 M) as precursor. The prepared scoria samples were dip coated in ZnO gel, according to our previous work<sup>18</sup>. This procedure was repeated four times and after each run, the film was dried at  $80^\circ\text{C}$  in an oven for 30 min to evaporate the solvent and then calcinated at  $400^\circ\text{C}$  for 2 h to achieve ZnO thin layer.

50 g of the prepared ZnO/scoria nanophotocatalyst was immersed in 100 ml of 20 mM  $\text{Cu}(\text{NO}_3)_2$  solution and shaken in a shaker-incubator (Fan Avarane Sahand Azar - Iran) for 1 h at  $22^\circ\text{C}$ . The granules were washed with distilled water and immersed in freshly prepared  $\text{NaBH}_4$  (20 mM) solution in water-ice bath ( $4^\circ\text{C}$ ) under vigorous stirring for 1 h to growth CuO thin film. During this step,

the samples became black indicating CuO film formation. The samples were taken out from the solution, rinsed with distilled water and dried at  $80^\circ\text{C}$  for 24 h.

The structural characterizations of ZnO /scoria and CuO/ZnO/scoria nanophotocatalysts were carried out by X-ray diffraction (XRD) analysis using a Simens D-500 (Germany) with Cu  $K_\alpha$  radiation at a wavelength of 0.15406 nm. The morphologies of ZnO/scoria and CuO/ZnO/scoria nanophotocatalysts were studied by a scanning electron microscope (SEM) (MIRA3 FEG-SEM Tescan, Czech). Energy dispersive X-ray spectroscopy (EDS) was used to confirm the syntheses of ZnO/scoria and CuO/ZnO/scoria nanophotocatalysts using a MIRA3 Tescan (Czech). Also, the chemical composition of the scoria was studied by X-ray fluorescence (XRF) analysis (Philips PW 2404, Netherlands). The optical absorbances of ZnO/scoria and CuO/ZnO/scoria samples were recorded using a diffuse reflectance spectrometer (DRS) (Sinco S4100, Korea). Surface area of scoria, ZnO/scoria and CuO/ZnO/scoria was obtained through the Brunauer–Emmett–Teller (BET) with micromeritics Gemini 2375 (USA) analyzer.

### 2.6. Experimental set-up

Fig. 1 illustrates the schematic of the photoreactor used for AB113 decolorization in this research. The rectangular photoreactor was made of Plexiglass with the dimensions of  $20 \times 8 \times 8$  cm and effective volume of 350 ml. In the bottom of the photoreactor a reticulated sheet was placed and it was covered by 160 g CuO/ZnO/scoria samples. Four 3-W power LED lamps (Manai Co., Iran) with intense emission lines at 460 and 550 nm were used as irradiation source (Fig.2). The distance between lamps and the solution surface was 7 cm. A vertical baffle was placed in the inlet of the photoreactor to avoid from the canalization of the feed solution. AB113 solution was fed into the reactor through a pump and its flow was adjusted using a flow meter, and LED lamps irradiated the solution. AB113 samples were withdrawn every 15 min and decolorization efficiency was calculated spectrophotometrically according to Eq (1). Effect of different variables, i.e. pH, feed flow rate, AB113 concentration and coexisting anions were investigated. For real textile wastewater, samples were withdrawn after 1.5 h treatment and analyzed by COD measurement (Eq. 2).

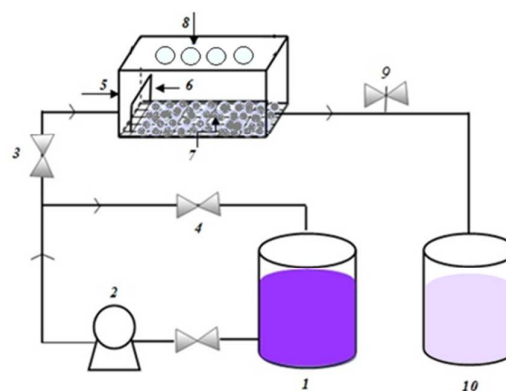


Fig.1. Experimental set up. (1) Reservoir, (2) Pump, (3) Inlet valve, (4) By pass valve, (5) Photoreactor, (6) Baffle, (7) Granular CuO/ZnO/scoria samples, (8) LED lamps, (9) Sampling valve and (10) Treated water reservoir.

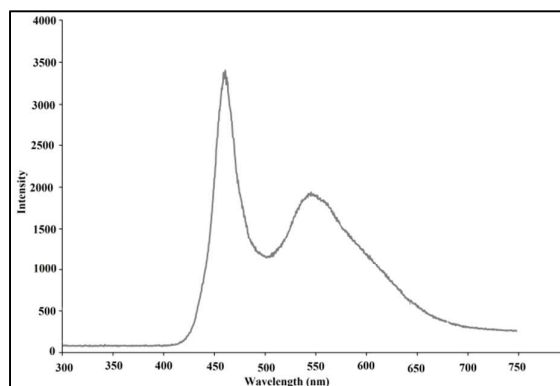


Fig. 2. Emission spectrum of the visible power LED lamp.

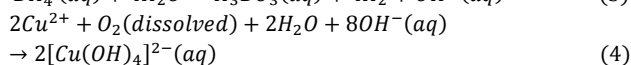
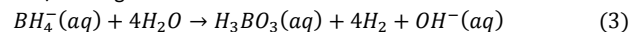
### 2.7. Point of zero charge of CuO /ZnO/ scoria samples

To determine the point of zero charge (PZC) of CuO/ZnO/scoria samples, 40-ml samples of  $\text{NaNO}_3$  solution (0.1 M) were prepared with different pH values.  $\text{HNO}_3$  and  $\text{NaOH}$  solutions (0.1 and 0.5 M) and a pH meter (Eutech pH 510, Malaysia) were used to adjust the pH values between 2 and 11. Powdered CuO/ZnO/scoria samples (0.2 g) were added to each solution. The solutions were shaken for 24 h in a shaker-incubator at 20 °C. The final pH of each solution was recorded and  $\Delta\text{pH}$  values (the difference between initial and final pH of the solutions) were plotted against initial pH (pHi) values. The PZC was the pH value at which  $\Delta\text{pH}$  was equal to zero<sup>19, 20</sup>.

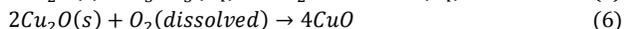
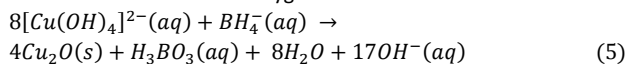
## 3. Results and discussion

### 3.1. Synthesis of CuO/ZnO/scoria

In this research  $\text{NaBH}_4$  was used as alkalization and reducing reagent of  $\text{Cu}^{2+}$ . The chemical reactions of CuO preparation on ZnO/scoria granules are as follows<sup>21</sup>:



$\text{NaBH}_4$  further reduces  $[\text{Cu}(\text{OH})_4]^{2-}$  complex into  $\text{Cu}_2\text{O}$  and finally  $\text{Cu}_2\text{O}$  crystals are converted to CuO through a slow oxidation by trace amount of dissolved oxygen.



Also, the chemical bonds of  $-\text{Zn}-\text{O}-\text{Cu}-$  takes place at the surface of ZnO/scoria to make the CuO/ZnO/scoria.

### 3.2. Characteristics of CuO/ZnO/scoria samples

The chemical compositions of the scoria, ZnO/scoria, and CuO/ZnO/scoria samples were determined by XRF analysis. According to the obtained results scoria mainly consist of  $\text{SiO}_2$  (41.6%),  $\text{Al}_2\text{O}_3$  (12.9%) and  $\text{Fe}_2\text{O}_3$  (8.5%). Percentage of ZnO and CuO on ZnO/scoria and CuO/ZnO/scoria were obtained 4.2% and 0.5% respectively (Table 1).

Table 1. Chemical composition of scoria, ZnO/scoria, and CuO/ZnO/scoria samples by XRF analysis.

Material	Scoria	ZnO /scoria	CuO/ZnO /Scoria
$\text{SiO}_2$	46.1	45.2	45.1
$\text{Al}_2\text{O}_3$	12.9	12.6	12.5
$\text{Fe}_2\text{O}_3$	8.5	8.2	8.2
$\text{CaO}$	8.2	8.0	8.0
$\text{Na}_2\text{O}$	7.7	7.3	7.25
$\text{MgO}$	6.5	6.3	6.3
$\text{K}_2\text{O}$	4.3	4.1	4.1
$\text{TiO}_2$	1.6	1.5	1.4
$\text{ZnO}$	0.00	4.20	4.20
$\text{CuO}$	0.00	0.00	0.50
Others	4.2	2.6	2.45

In order to determine the composition of the synthesized nanophotocatalysts, qualitative analysis of XRD patterns was performed using the Xpert High Score software and the JCPDS PDF-2 database. The XRD patterns of scoria, ZnO/scoria and CuO/ZnO/scoria samples have been depicted in Fig. 3 (a, b, and c respectively). ZnO/scoria and CuO/ZnO/scoria patterns show the peaks related to scoria in comparison with single scoria pattern. Also these patterns show ZnO and ZnO/CuO peaks that are consistent with the standard data given in JCPDS cards (00-001-1136) and (00-001-1117), respectively. These results approve the synthesis and immobilization of ZnO and CuO nanoparticles on scoria.

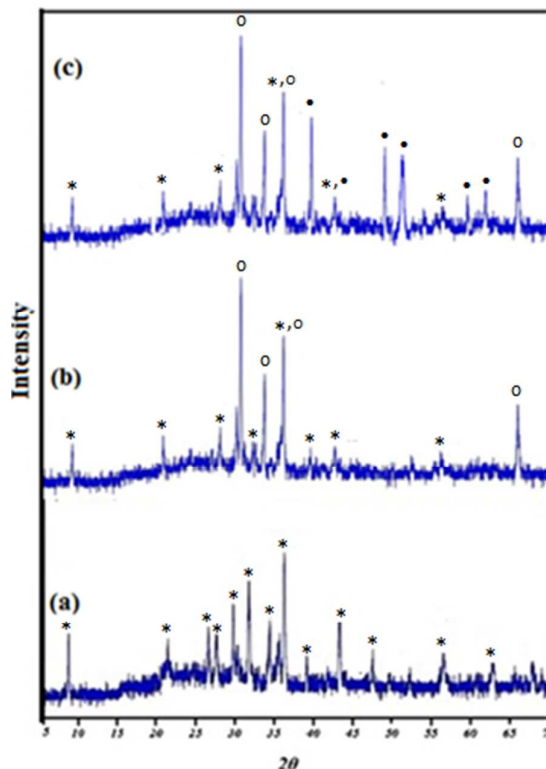


Fig. 3: XRD patterns of (a) scoria, (b) ZnO/scoria and (c) CuO/ZnO/scoria samples. \*, o, • represent scoria, ZnO and CuO respectively.

The EDS plots of ZnO/scoria and CuO/ZnO/scoria samples have been shown in Fig. 4 (a and b, respectively). X-ray energies equal to 1.43 and 1.64 KeV at both samples, are related to  $\text{Al}_2\text{O}_3$  and  $\text{SiO}_2$ , respectively which are the main constituents of scoria<sup>22</sup>. For ZnO/scoria, the main X-ray energies of 0.59 and 1.04 KeV represent the emissions from the K-shell of oxygen and L-shell of zinc, respectively<sup>23</sup>. These energies confirm ZnO synthesis and its immobilization on the scoria. In Fig. 4 (b), in addition to the energy peaks of scoria and ZnO, the peaks at 0.95, 8.12 and 9.0 KeV are related to Cu and confirm the synthesis of CuO on ZnO/scoria.

Fig. 5 shows the SEM images of scoria, scoria/ZnO and CuO/ZnO/scoria samples. Porous surface of scoria rocks can be seen in Fig. 5a. Uniform immobilization of ZnO on scoria can be seen in Fig. 4b with the average size of 40 nm. Synthesis of CuO nanoparticles on ZnO/scoria with average size of 30 nm can be seen in Fig. 5c. The cross sectional SEM image of CuO/ZnO/scoria photocatalyst has been depicted in Fig. 5d. Using this figure the approximate thickness of CuO/ZnO was estimated 800 nm.

Fig. 6 illustrates the elemental EDS mapping of CuO/ZnO/scoria photocatalyst. Results of this analysis indicate the uniform immobilization of ZnO on scoria surface. Uniform doping of ZnO/scoria with CuO was confirmed by Fig. 6d, too.

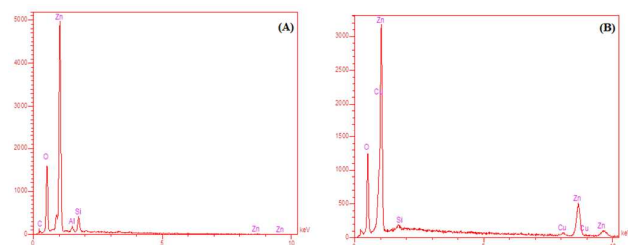


Fig. 4: EDS analysis of (a) ZnO/scoria and (b) CuO/ZnO/scoria samples.

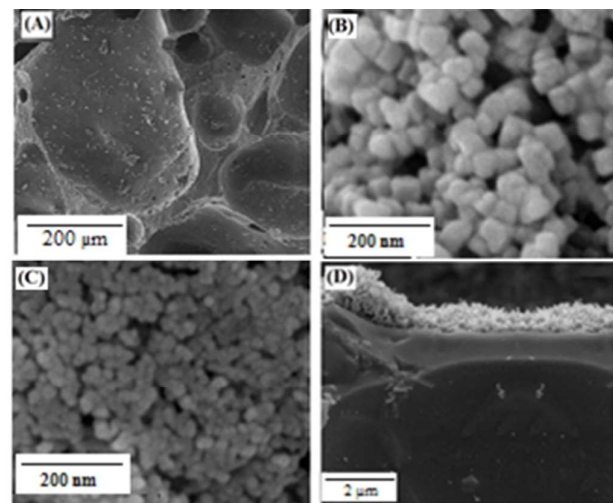


Fig. 5: SEM image of scoria (A), ZnO/scoria (B), CuO/ZnO/scoria (C), and crossing section of CuO/ZnO/scoria (D).

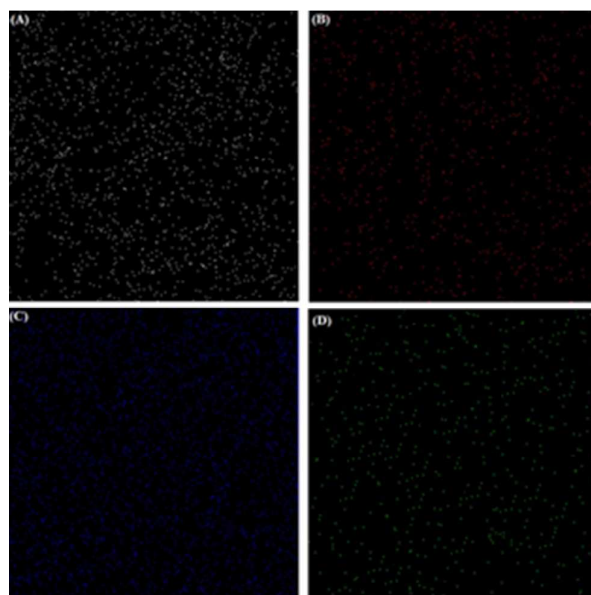


Fig. 6: Elemental mapping of CuO/ZnO/scoria, (A) oxygen, (B) Si, (C) Zn, and (D) Cu.

The optical absorbance of the scoria, prepared ZnO/scoria and CuO/ZnO/scoria samples were recorded by diffuse reflectance spectrometer (Fig. 7). DRS spectra of the photocatalysts indicate that both of the samples have similar absorbance values at UV region. But in visible region (>420 nm) CuO/ZnO/scoria shows higher absorbance compared with ZnO/scoria due to the presence of CuO nanoparticles. It is obvious that the presence of CuO in nanophotocatalyst increases its photocatalytic activity under visible light and makes it suitable for application under visible light irradiation. DRS spectrum of scoria in compared with ZnO/scoria and CuO/ZnO/scoria shows low absorbance at UV and visible regions.

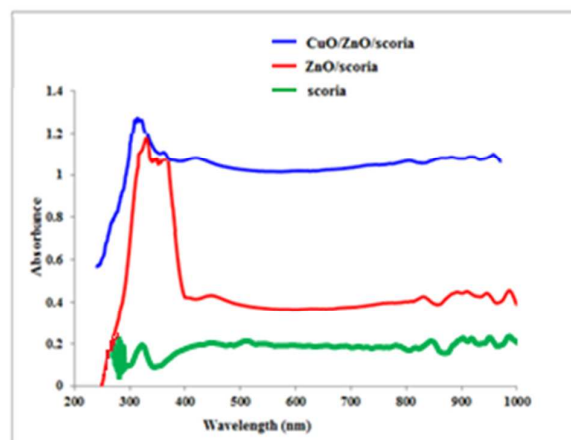


Fig. 7: Diffuse reflectance spectra of scoria, ZnO/scoria and CuO/ZnO/scoria samples.

The surface area of the scoria calculated from the nitrogen isotherm using the BET method was  $1.65 \text{ m}^2 \text{ g}^{-1}$ . By the synthesis of ZnO on scoria the surface area is increased to  $9.49 \text{ m}^2 \text{ g}^{-1}$  and by

addition of CuO on ZnO/scoria it is increased to  $12.85 \text{ m}^2 \text{ g}^{-1}$ . These results are because of the addition of nanoparticles with high surface area. The high surface area enhances the photocatalytic activity of CuO/ZnO/scoria.

### 3.3. AB 113 decolorization efficiency by CuO/ZnO/scoria photocatalyst

The sole adsorption of AB113 on CuO/ZnO/scoria and also its sole photodegradation by visible light were insignificant compared with CuO/ZnO/scoria/Vis process as can be seen in Fig. 8. The results indicated that both of the irradiation and photocatalyst were necessary for the effective removal of the AB113<sup>24</sup>. Visible irradiation which reaches to the nanophotocatalyst surface leads to the formation of reactive hydroxyl radicals (Fig. 8).  $\cdot\text{OH}$ , with high oxidizing potential, leads to the final degradation of organic compounds to  $\text{CO}_2$ ,  $\text{N}_2$  and  $\text{H}_2\text{O}$ <sup>25,26</sup>.

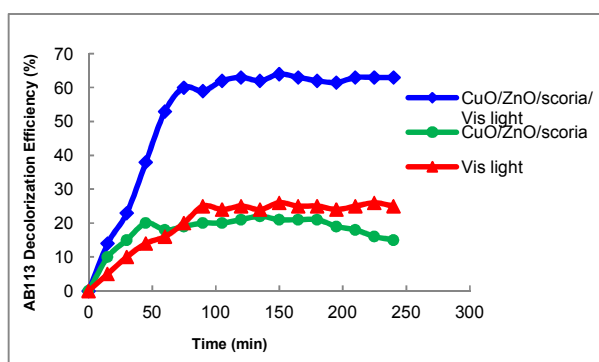


Fig. 8: Comparison of different methods of AB113 decolorization. (pH=5.0, effluent flow rate=15 ml min<sup>-1</sup>, initial dye concentration=20 mg L<sup>-1</sup>).

The schematic mechanism of photocatalytic dye removal process through the immobilized CuO/ZnO nanocomposite on the scoria under visible light irradiation is demonstrated in Fig. 9. In the presence of ZnO/CuO composite the interfacial charge transfer between these semiconductors leads to high efficiency of photocatalytic process under visible light irradiation. Because of low band gap energy, it is assumed that photon of visible irradiation excites electron from valence band of CuO to the conduction band, leaving holes in the valence band. The produced electrons in the conduction band of CuO jump to the conduction band of ZnO, while the electrons from valence band of ZnO transfer to the valence band of CuO<sup>27</sup>. This helps to inhibit the recombination of electrons and holes and consequently improves the charge separation and dye removal efficiency.

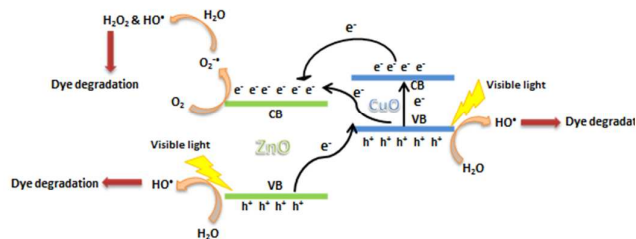
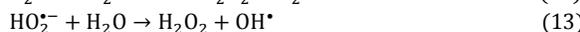
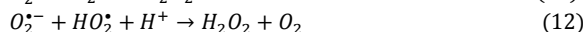
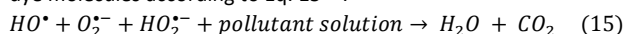


Fig. 9: Schematic mechanism of photocatalytic process through the immobilized CuO/ZnO nanocomposite on the scoria under visible light irradiation.

Various mechanisms of the production of  $\cdot\text{OH}$  and other active radicals in this process are summarized below<sup>28,29</sup>.



Finally, the reactive radicals especially hydroxyl radical, degrade the dye molecules according to Eq. 15<sup>30</sup>:



### 3.4. Investigation of effective parameters

#### 3.4.1. Effect of pH on AB113 decolorization

pH of dye solution is an important parameter in photocatalytic processes. To study the effect of pH, AB113 decolorization experiments were performed at pH values of 3.0, 4.5, 6.0, 7.5, and, 9.0 while CuO/ZnO/scoria sample mass, AB113 initial concentration and effluent flow rate were constant at 160 g, 20 mg L<sup>-1</sup> and 15 ml min<sup>-1</sup>, respectively. As can be seen in Fig. 10 (a), decolorization efficiency was higher at pH 4.5.

The effect of initial pH of dye solution on decolorization efficiency depends on the anionic or cationic nature of dye molecules and the point of zero charge (PZC) of photocatalyst<sup>25, 31, 32</sup>. The PZC of CuO/ZnO/scoria nanophotocatalyst is equal to 6.70 (Fig. 10 b), therefore the photocatalyst surface charge is positive at pH values lower than 6.70 while it is negative at higher pH values. The electrostatic interaction between AB113 and the surface of the photocatalyst is higher at pH values lower than 6.70, due to the anionic structure of AB113. According to the figure, the highest positive surface charge can be seen at pH=4.5 and so, it shows the highest decolorization efficiency. The lower efficiency of AB113 decolorization at pH 3 may be attributed to the dissolution of ZnO at acidic pHs<sup>24</sup>.

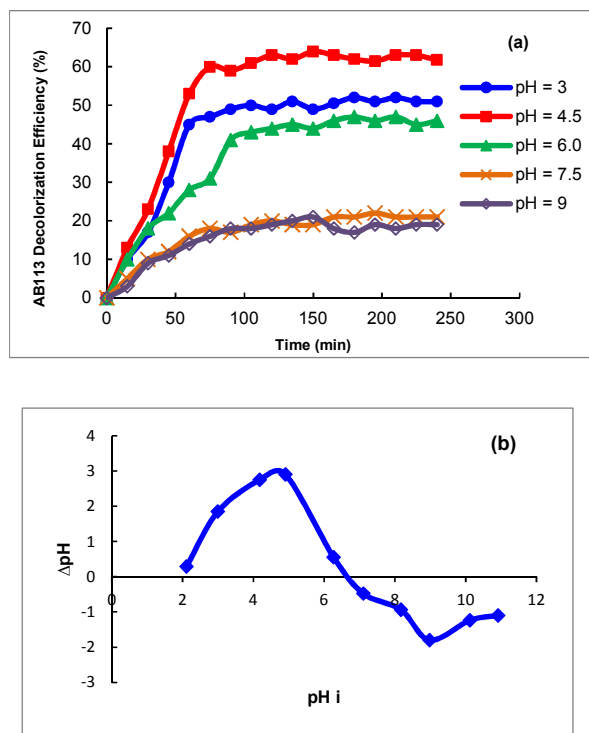


Fig. 10: (a) Effect of pH on AB113 decolorization efficiency using CuO/ZnO/scoria nanophotocatalyst (nanophotocatalyst dose= 160 g, flow rate= 15 ml min<sup>-1</sup>, initial dye concentration=20 mgL<sup>-1</sup>), (b) Plot of ΔpH vs. initial pH to obtain the PZC of CuO/ZnO/scoria samples (T= 20 °C, agitation rate= 150 rpm, t= 24 h).

#### 3.4.2. Effect of effluent flow rate on AB113 decolorization

The dye solution flow rate is an important parameter in decolorization process because it changes the residence time of dye molecules in the photoreactor. Flow rate was varied in the range of 5-25 ml min<sup>-1</sup> in this study. High residence times and subsequently low flow rates lead to more <sup>•</sup>OH generation and higher decolorization (Fig. 11).

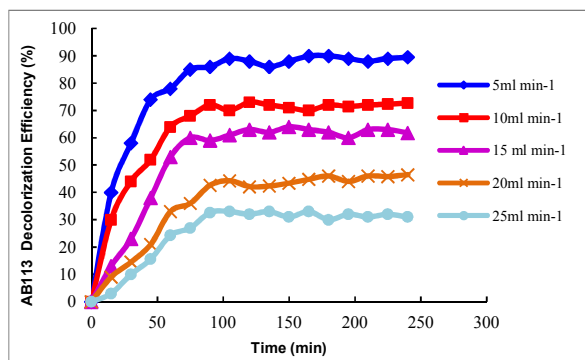


Fig. 11: Effect of AB113 solution flow rate on its decolorization using CuO/ZnO/scoria nanophotocatalyst. (nanophotocatalyst dose=160 g, pH= 5.0, initial dye concentration=20 mgL<sup>-1</sup>).

#### 3.4.3. Effect of initial AB113 concentration on its decolorization

Initial AB113 concentration was varied in the range of 5–40 mg L<sup>-1</sup>. The decolorization efficiency decreased with increasing initial concentration of the dye solution as can be seen in Fig. 12. Increasing dye concentration decreases light penetration in the solution and the irradiation of photocatalyst surface and consequently, the generation of <sup>•</sup>OH is reduced. Also, photocatalytic surface sites are limited<sup>33,34</sup>. Therefore by increasing dye concentration, the number of its molecules increases while the number of photocatalytic sites is constant.

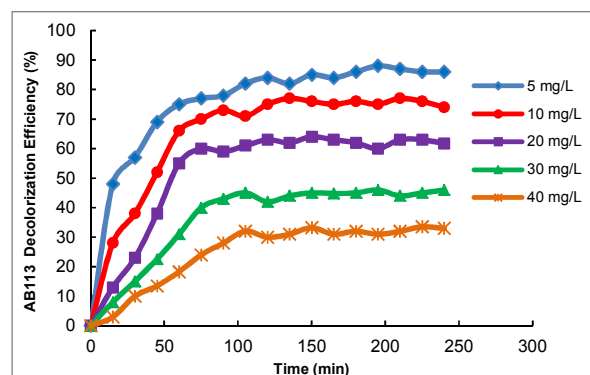


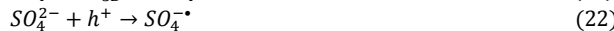
Fig. 12: Effect of initial AB113 concentration on its decolorization using CuO/ZnO/scoria nanophotocatalyst. Nanophotocatalyst dose=160 g, pH=5.0, flow rate=15 ml min<sup>-1</sup>.

#### 3.4.4. Effect of coexisting anions on AB113 decolorization

Anions such as SO<sub>4</sub><sup>2-</sup>, Cl<sup>-</sup> and NO<sub>3</sub><sup>-</sup> are common constituents of wastewaters. They may influence the photocatalytic processes and degradation efficiency of organic pollutants<sup>35</sup>. Chloride anion is adsorbed on photocatalyst surface and occupies the photocatalytic sites and therefore, it has negative effect on decolorization efficiency. In addition, it scavenges the positive holes and <sup>•</sup>OH via the following reactions<sup>36</sup>.



Sulphate similar to chloride has negative effect on decolorization efficiency. It acts as the scavenger of positive holes and <sup>•</sup>OH according to the following reactions<sup>37</sup>.



Nitrate shows the least negative effect on AB113 photocatalytic decolorization efficiency as can be seen in Fig. 13. Yajun et al.<sup>38</sup> found a similar result in methyl orange decolorization using polyoxometalate as photocatalyst with the least inhibition effect for nitrate compared with chloride and sulfate: Cl<sup>-</sup> > SO<sub>4</sub><sup>2-</sup> > NO<sub>3</sub><sup>-</sup>.

According to Fig. 13, anions have negative effect on decolorization efficiency with the order of Cl<sup>-</sup> > SO<sub>4</sub><sup>2-</sup> > NO<sub>3</sub><sup>-</sup>. As a conclusion, the presence of these anions in water or wastewater decreases the efficiency of photocatalytic decolorization.

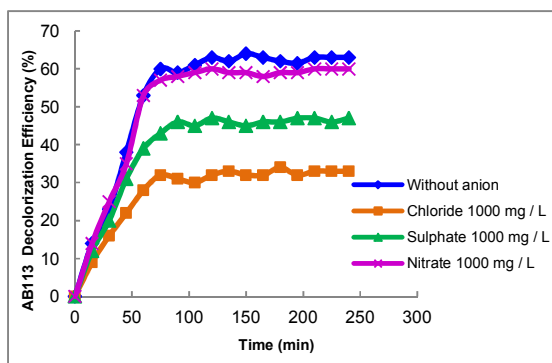


Fig. 13: Effect of coexisting anions on AB113 decolorization using CuO/ZnO/scoria nanophotocatalyst. Nanophotocatalyst dose=160 g, pH=5.0, initial dye concentration=20 mgL<sup>-1</sup>, flow rate=15 ml min<sup>-1</sup>.

### 3.4.5. Effect of pH on real textile wastewater treatment

Effect of pH of real textile wastewater was studied in 3 levels (4, 7 and 10) while its initial COD was 700 mg/L and wastewater flow rate was 5 ml/min. As can be seen in Fig. 14a, the visible range absorbance of the wastewater decreases confirming the degradation of dye molecules of the wastewater. pH 4 showed the highest decrease in solution absorbance with the highest COD removal efficiency of 47% (Fig. 14b). This behavior could be justified similar to that of AB113 solution, discussed in section 3.4.1.

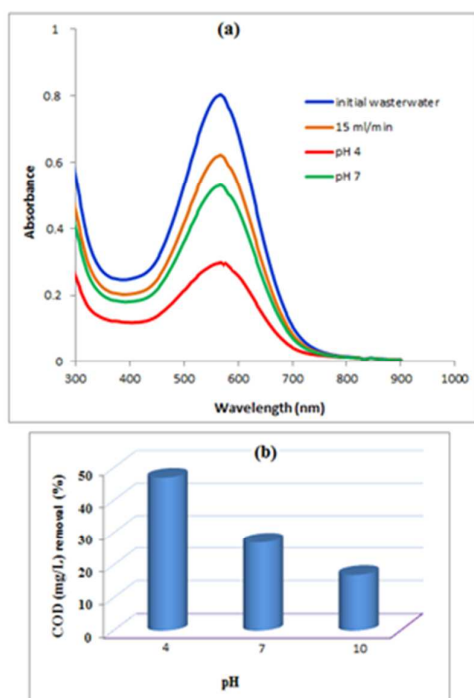


Fig. 14: Effect of pH of the real textile wastewater on (a) absorbance spectra and (b) COD removal. (Flow rate=5 ml min<sup>-1</sup>, initial COD=700 mgL<sup>-1</sup>).

### 3.4.6. Effect of flow rate on real textile wastewater treatment

Effect of effluent flow rate (2, 5, 10 and 15 ml min<sup>-1</sup>) on real textile wastewater treatment at initial COD of 700 mg/L and pH 4 has been shown in Fig. 15 (a) and (b). According to these Figs., the more the flow rate was, the more decrease in COD removal efficiency was seen. This behavior could be justified similar to that of AB113 solution, discussed previously in section 3.4.2.

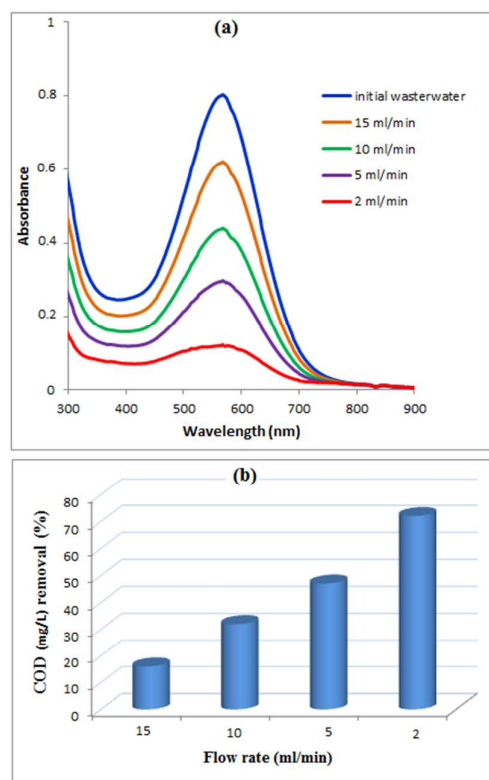


Fig. 15: Effect of flow rate of the real textile wastewater on (a) absorbance spectra and (b) COD removal. (pH=4 and initial COD=700 mgL<sup>-1</sup>)

### 3.5. Reusability of CuO/ZnO/scoria nanophotocatalyst

CuO/ZnO/scoria nanophotocatalyst was used for AB113 decolorization and textile wastewater treatment for five consecutive cycles to study its reusability. After each run, the used catalyst was regenerated using visible light irradiation for 2 h in distilled water to eliminate the organic molecules and then by drying at 80°C in an oven. The results are illustrated in Fig. 16. The results show insignificant decrease in the efficiency of decolorization and COD removal and so the samples have good reusability. As can be seen from this figure, AB 113 decolorization and COD removal were decreased 2.9% and 4.0% respectively after 5 cycle.

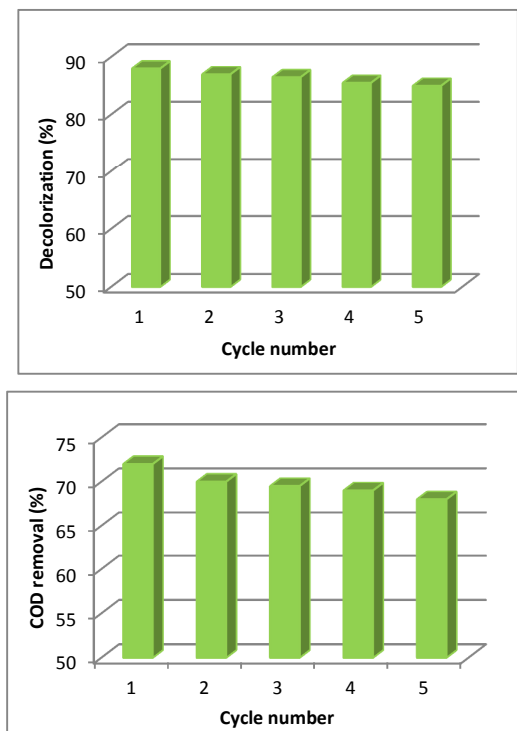


Fig. 16: The reusability of CuO/ZnO/scoria nanophotocatalyst within five consecutive cycles (a) decolorization efficiency (nanophotocatalyst dose=160 g, pH=5.0, initial dye concentration=20 mgL<sup>-1</sup>, flow rate=15 ml min<sup>-1</sup>), and (b) COD removal from wastewater (pH=4.0, Flow rate=2 ml min<sup>-1</sup>, initial COD=700 mgL<sup>-1</sup>).

### Conclusion

Thin film of ZnO was synthesized successfully on scoria by sol-gel and dip-coating method. CuO was synthesized on ZnO/scoria by direct crystallization using NaBH<sub>4</sub>. According to XRD, EDS and SEM analyses CuO synthesis was successful on ZnO/scoria. According to the DRS results, CuO/ZnO/scoria nanophotocatalyst has higher absorbance in visible region than ZnO/scoria. The synthesized CuO/ZnO/scoria proved to be a potential photocatalyst for decolorization of Acid Blue 113 and treatment of a real textile wastewater under visible light irradiation. According to the results, AB113 solution decolorization efficiency is dependent on pH, its initial concentration, flow rate and coexisting anions (Cl<sup>-</sup> and SO<sub>4</sub><sup>2-</sup>), and the COD removal efficiency of the real textile wastewater depends on its pH and flow rate.

### Acknowledgment

This paper is published as part of a research project supported by the University of Tabriz Research Affairs Office. The authors like to express their gratitude to the University of Tabriz for financial and other supports provided in the implementation of this research project.

### References

1. J. Miao, Z. Jia, H.B. Lu, D. Habibi and L.-C. Zhang, *Journal of the Taiwan Institute of Chemical Engineers*, 2014, **45**, 1636-1641.
2. S. Aber, R. Soltani-Jigheh and A. R. Khataee, *Desalination and Water Treatment*, 2014, 1-8.
3. B. Subash, B. Krishnakumar, V. Pandiyan, M. Swaminathan and M. Shanthi, *Materials Research Bulletin*, 2013, **48**, 63-69.
4. M. Pirhashemi and A. Habibi-Yangjeh, *Applied Surface Science*, 2013, **283**, 1080-1088.
5. B. Ayoubi-Feiz, S. Aber, A. Khataee and E. Alipour, *Journal of Molecular Catalysis A: Chemical*, 2014, **395**, 440-448.
6. B. Ayoubi-Feiz, S. Aber and M. Sheydaei, *RSC Advances*, 2015, **5**, 19368-19378.
7. P. Senthil Kumar, M. Selvakumar, P. Bhagabati, B. Bharathi, S. Karuthapandian and S. Balakumar, *RSC Advances*, 2014, 32977-32986.
8. B. P. Nenavathu, A. V. R. Krishna Rao, A. Goyal, A. Kapoor and R. K. Dutta, *Applied Catalysis A: General*, 2013, **459**, 106-113.
9. A. Hamrouni, H. Lachheb and A. Houas, *Materials Science and Engineering: B*, 2013, **178**, 1371-1379.
10. Y. Yang, Y.Q. Li, H.Q. Shi, W.N. Li, H.M. Xiao, L.P. Zhu, Y.S. Luo, S.Y. Fu and T. Liu, *Composites Part B: Engineering*, 2011, **42**, 2105-2110.
11. Y. Liu, L. Sun, J. Wu, T. Fang, R. Cai and A. Wei, *Materials Science and Engineering: B*, 2015, **194**, 9-13.
12. S. Adhikari, D. Sarkar and G. Madras, *RSC Advances*, 2015, **5**, 11895-11904.
13. G. Xiaoyan, Z. Xiaojie, T. Yincai, H. Yabei, Y. Zhang and Z. Yanqin, *Kinet Catal*, 2011, **52**, 672-677.
14. J.-S. Kwon, S.T. Yun, J.H. Lee, S.O. Kim and H. Y. Jo, *Journal of Hazardous Materials*, 2010, **174**, 307-313.
15. M. Kitis, S. S. Kaplan, E. Karakaya, N. O. Yigit and G. Civelekoglu, *Chemosphere*, 2007, **66**, 130-138.
16. M. Sheydaei, S. Aber and A. Khataee, *Journal of Industrial and Engineering Chemistry*, 2014, **20**, 1772-1778.
17. P. Jongnavakit, P. Amornpitoksuk, S. Suwanboon and T. Ratana, *Thin Solid Films*, 2012, **520**, 5561-5567.
18. F. Mahdizadeh, S. Aber and A. Karimi, *Journal of the Taiwan Institute of Chemical Engineers*, 2015, **49**, 212-219.
19. S. Mustafa, B. Dilara, K. Nargis, A. Naeem and P. Shahida, *Colloids and Surfaces A: Physicochemical and Engineering Aspects*, 2002, **205**, 273-282.
20. M. Sheydaei and S. Aber, *CLEAN – Soil, Air, Water*, 2013, **41**, 890-898.
21. G. Fan and F. Li, *Chemical Engineering Journal*, 2011, **167**, 388-396.

22. B. Yahyaei, S. Azizian, A. Mohammadzadeh and M. Pajohi-Alamoti, *Chemical Engineering Journal*, 2014, **247**, 16-24.
23. R. Zamiri, B. Singh, I. Bdkin, A. Rebelo, M. Scott Belsley and J. M. F. Ferreira, *Solid State Communications*, 2014, **195**, 74-79.
24. M. A. Behnajady, N. Modirshahla and R. Hamzavi, *Journal of Hazardous Materials*, 2006, **133**, 226-232.
25. N. Daneshvar, S. Aber, M. S. Seyed Dorraji, A. R. Khataee and M. H. Rasoulifard, *Separation and Purification Technology*, 2007, **58**, 91-98.
26. A. A. Khodja, T. Sehili, J. Pilichowski and P. Boule, *Journal of Photochemistry and Photobiology A: Chemistry*, 2001, **141**, 231-239.
27. Sini Kuriakose, D. K. Avasthi and Satyabrata Mohapatra, *Beilstein Journal of Nanotechnology* 2015, **6**, 928-937.
28. X. Wang, J. Wang, Z. Cui, S. Wang and M. Cao, *RSC Advances*, 2014, **4**, 34387.
29. A. Yousef, N. A. M. Barakat, T. Amna, A. R. Unnithan, S. S. Al-Deyab and H. Yong Kim, *Journal of Luminescence*, 2012, **132**, 1668-1677.
30. I. k. Konstantinou and T. A. Albanis, *Applied Catalyst B: Environment*, 2004, **49**, 1-14.
31. A. Shafaei, M. Nikazar and M. Arami, *Desalination*, 2010, **252**, 8-16.
32. J. Xia, A. Wang, X. Liu and Z. Su, *Applied Surface Science*, 2011, **257**, 9724-9732.
33. M. Muruganandham, N. Shobana and M. Swaminathan, *Journal of Molecular Catalysis A: Chemical*, 2006, **246**, 154-161.
34. A. Nageswara Rao, B. Sivasankar and V. Sadasivam, *Journal of Hazardous Materials*, 2009, **166**, 1357-1361.
35. S. Chen and Y. Liu, *Chemosphere*, 2007, **67**, 1010-1017.
36. D. E. Santiago, J. Araña, O. González-Díaz, M. E. Alemán-Dominguez, A. C. Acosta-Dacal, C. Fernandez-Rodríguez, J. Pérez-Peña and J. M. Doña-Rodríguez, *Applied Catalysis B: Environmental*, 2014, **156-157**, 284-292.
37. N. M. Mahmoodi, M. Arami and J. Zhang, *Journal of Alloys and Compounds*, 2011, **509**, 4754-4764.
38. D G Rao, R Senthikumar, J Anthony Byrne and S Feroz, *Wastewater Treatment: Advanced Processes and Technologies*, CRC Press, 2012.